THE ASTROPHYSICAL JOURNAL, 544:843–858, 2000 December 1

INFRARED SPECTROSCOPY OF MOLECULAR SUPERNOVA REMNANTS

WILLIAM T. REACH AND JEONGHEE RHO
Infrared Processing and Analysis Center, California Institute of Technology, Pasadena, CA 91125; reach@ipac.caltech.edu
Received 2000 April 20; accepted 2000 July 13

ABSTRACT

We present *Infrared Space Observatory* spectroscopy of sites in the supernova remnants W28, W44, and 3C 391, where blast waves are impacting molecular clouds. The complete wavelength range from 42 to 188 μm was observed with the Long Wavelength Spectrometer, as well as narrow ranges centered on 4.695, 9.665, 25.98, and 34.82 μm with the Short Wavelength Spectrometer. Atomic fine-structure lines were detected from (in order of atomic number): C^+, N^+, N^{++}, O^0, O^{++}, O^{+++}, Si^+, P^+, and Fe^+. The two lines of H_2 that we observed, $S(3)$ and $S(9)$, were detected for all three remnants. The observations require both shocks into gas with moderate ($\sim 10^2$ cm^{-3}) and high ($\sim 10^4$ cm^{-3}) preshock densities, with the moderate-density shocks producing the ionic lines and the high-density shock producing the molecular lines. No single shock model can account for all of the observed lines, even at the order of magnitude level. We find that the principal coolants of radiative supernova shocks in moderate-density gas are the far-infrared continuum from dust grains surviving the shock, followed by collisionally excited [O I] 63.2 μm and [Si II] 34.8 μm lines. The principal coolant of the high-density shocks is collisionally excited H_2 rotational and ro-vibrational line emission. We systematically examine the ground-state fine structure of all cosmically abundant elements to explain the presence or lack of all atomic fine lines in our spectra in terms of the atomic structure, interstellar abundances, and a moderate-density, partially ionized plasma. The [P II] line at 60.6 μm is the first known astronomical detection, but its brightness can be explained using the solar abundance of P. There is only one, bright unidentified line in our spectra, at 74.26 μm; as there is no plausible atomic fine-structure line at this wavelength, we suggest this line is molecular. The presence of bright [Si II] and [Fe II] lines requires partial destruction of the dust. The required gas-phase abundance of Fe suggests 15%–30% of the Fe-bearing grains were destroyed. Adding the Si and Fe gas mass, and correcting for the mass of other elements normally found in dust, we find $\sim 0.5\ M_\odot$ of dust vapors from the shocked clump 3C 391:BML. The infrared continuum brightness requires $\sim 1\ M_\odot$ of dust survives the shock, suggesting about 1/3 of the dust mass was destroyed, in agreement with the depletion estimate and with theoretical models for dust destruction.

Subject headings: infrared: ISM: lines and bands — ISM: abundances — line: identification — shock waves — supernova remnants

1. INTRODUCTION

Infrared spectroscopy is a particularly useful tool for studying supernova remnants (and other shocks) in dense gas for the following reasons. (1) Infrared atomic fine-structure lines are produced by gas with the physical conditions expected behind radiative shocks. Dense, shocked gas rapidly cools to temperatures of 10^2–10^3 K, where infrared transitions are excited. This cool layer dominates the shocked column density, while the layer that emits optical to X-ray lines is extremely narrow. The kinetic temperature of the cooling postshock gas is perfectly suited to the energy levels of infrared fine-structure lines from atoms and ions and infrared vibrational, ro-vibrational, and quadrupole vibrational (H_2) lines from molecules. (2) Infrared fine-structure lines trace the ground-state populations of the all of the abundant elements that have electronic ground states with nonzero angular momentum. By measuring the brightness of transitions directly to the ground state or within a narrow multiplet of energy levels including the ground state, a reasonably accurate measure of the column density of each species can be determined. Using pairs of lines from different elements due to energy levels with similar spacings, it is possible to measure relative abundances with confidence. (3) Far-infrared fine-structure lines are not affected by extinction. The light produced by postshock gas is significantly affected by extinction from dust in the preshock cloud and the intervening medium along the line of sight. Extinction effects are severe in the ultraviolet and also in the optical and near-infrared for inner-galaxy supernova remnants, where the line-of-sight column density often exceeds 10^{22} cm^{-2}, but extinction is negligible in the far-infrared. Many supernova remnants interacting with clouds are known only from their radio or hard X-ray emission, despite being copious producers of soft X-rays and optical line emission, because they are too distant or they are within or behind a molecular cloud.

Recent advances in infrared astronomy have opened the far-infrared window to spectroscopy of faint emission. The observations used in this paper were made with the Long-Wavelength Spectrometer (LWS; Clegg et al. 1996) aboard the *Infrared Space Observatory* (*ISO*; Kessler et al. 1996), whose mission lasted from 1996 to 1997. A complete spectrum with the LWS, covering the 40–190 μm wavelength region with a resolution of 0.29–0.6 μm, took less than half an hour to reach a sensitivity adequate to detect atomic fine-structure lines and molecular rotational lines for a variety of astronomical sources. Instruments planned for the Stratospheric Observatory for Infrared Astronomy (SOFIA; Becklin 1997; expected to begin observing in 2002) will open opportunities for far-infrared spectroscopic observations over most of the far-infrared wavelength range—specifically, the part not affected by absorption and emission by very abundant molecules in the residual atmosphere such as H_2O. In the somewhat more distant future,

instruments aboard the Far-Infrared Space Telescope (FIRST; Poglitsch 1997; anticipated launch 2007) will allow continuous spectral coverage to even deeper levels for extended sources.

The goal of this paper is to present our *ISO* LWS and SWS spectral observations of the molecular supernova remnants W44, W28, and 3C 391 and to illustrate from basic physical principles why the spectral lines we detected are bright. Shocked gas in supernova remnants emits virtually all fine-structure lines from the abundant elements. We show the inferred elemental abundances after impact from the supernova shock, and we discuss implication of grain destruction for elements such as Fe, Si, and P which were locked in grains.

This paper continues our investigation of infrared emission from molecular supernova remnants. The brightness of the [O I] 63.2 μm line for W44 and 3C 391 was presented in our first paper (Reach & Rho 1996). The far-infrared molecular emission of OH, CO, and H_2O was presented in the second paper (Reach & Rho 1998). The millimeter-wave molecular emission of CO, CS, HCO^+ was presented in the third paper for 3C 391 (Reach & Rho 1999), and in this paper we also present some molecular results for W44 from new IRAM 30 m observations. Two recent and closely related studies of molecular emission were presented by Seta et al. (1998) for W44 and Arikawa et al. (1999) for W28. The millimeter-wave observations show beyond doubt that all three of the supernova remnants discussed in this paper are interacting with molecular clouds.

2. OBSERVATIONS

2.1. *Far-Infrared Spectral Lines*

We obtained complete *ISO* LWS spectra of one position in each of three supernova remnants as part of our program of observing supernova-molecular cloud interactions (Reach & Rho 1996, 1998, 1999). The positions observed were the brightest OH masers (Frail et al. 1996) in W28 ($18^h01^m52^s.3$, $-23°19'25''$) and W44 ($18^h56^m28^s.4$, $+1°29'59''$) and the molecular peak in 3C 391:BML ($18^h49^m21^s.9$ $-0°57'22''$); all coordinates are J2000. Figure 1 shows the *ISO* LWS spectrum from 42 to 188 μm for all three remnants. For each of the 10 LWS detectors, we removed the fringes using the *ISO* Spectral Analysis Package[1] and subtracted a constant (due to residual dark current). Table 1 shows a list of the identified atomic fine-structure lines and their measured brightness. In order of atomic number, we detected atomic fine-structure lines from C^+, N^+, N^{++}, O^0, O^{++}, O^{+++}, and P^+ in the LWS spectra.

Part of the bright continuum and [C II] 157.7 μm line in Figure 1 are due to dust and gas along the line of sight, unrelated to the supernova remnant. At least part of the continuum is likely to be due to dust grains surviving the shocks. For example, for W44 we estimated 30% (Reach & Rho 1996) based on comparison to a reference position; a spectral analysis of the continuum is given in § 6 of this paper. To estimate the line-of-sight contamination of the spectral line brightnesses, we calculated the Galactic line-to-continuum ratio using the *COBE* Far-Infrared Absolute Spectrophotometer spectrum of the Galactic plane at longitude 30° (Reach et al. 1995). At the *ISO* LWS resolution, the expected line-to-continuum ratio due to unrelated gas for [C II] 157.7 μm is 2.2, while that for [N II] at 121.9 μm is 0.05. Comparing to our spectra, the 157.7 μm line to continuum ratios are 2.4, 1.2, and 1.9, and the 121.9 μm line to continuum ratios are 0.19, 0.09, and 0.16, for W44, W28, and 3C 391, respectively. Thus, much of the [C II] μm line emission could be due to line-of-sight gas, while only a small fraction the [N II] (and essentially none of the other lines) are due to line-of-sight gas. The subject of [C II] emission being related to the shock is addressed again in § 4, focusing on the abundance of C. An improved separation of the source and background brightness might be possible by analyzing the spatial variation of the brightness, which is beyond the scope of this paper.

2.2. *Mid-Infrared* Si, Fe, *and* H_2 *Lines*

We used the *ISO* SWS (de Graauw et al. 1996) to observe narrow ranges centered 25.98 and 34.82 μm for the ground-state transitions of [Fe II] and [Si II]. The spectra are shown in Figures 2 and 3, respectively. At the same time, we obtained spectra of the H_2 $S(9)$ and $S(3)$ lines; the spectra of these lines are shown in Figures 4 and 5, respectively. The brightnesses of the lines are summarized in Table 2. The SWS observations were toward the three lines of sight listed above, plus one extra position—toward the bright, northwestern radio ridge and a bright peak in the [O I] 63 μm strip map (position *b* in Fig. 3 of Reach & Rho 1996): 3C 391:radio ($18^h49^m19^s.4$, $-0°55'05''$). The two positions in 3C 391 have similar spectra of ionic fine-structure lines: the ratio of [Fe II]/[Si II] is nearly identical, although the [O IV] is relatively brighter toward 3C 391:radio by at least a factor of 3. In contrast, the brightness of the H_2 lines,

[1] The ISO Spectral Analysis Package (ISAP) is a joint development by the LWS and SWS Instrument Teams and Data Centers. Contributing institutes are CESR, IAS, IPAC, MPE, RAL, and SRON.

TABLE 1

OBSERVED FAR-INFRARED ATOMIC FINE-STRUCTURE LINES

ION	TRANSITION	WAVELENGTH	LINE BRIGHTNESS (10^{-4} ergs $s^{-1}cm^{-2}sr^{-1}$)		
			W28	W44	3C 391:BML
C^+	$^2P_{3/2\rightarrow1/2}$	157.741	7.77 ± 0.08	4.94 ± 0.04	6.54 ± 0.08
O^0	$^3P_{0\rightarrow1}$	145.525	0.75 ± 0.04	0.50 ± 0.03	0.90 ± 0.02
N^+	$^3P_{2\rightarrow1}$	121.898	0.68 ± 0.04	0.42 ± 0.04	0.89 ± 0.02
O^{++}	$^3P_{1\rightarrow0}$	88.356	0.38 ± 0.06	0.36 ± 0.02	1.49 ± 0.04
O^0	$^3P_{1-2}$	63.184	9.48 ± 0.02	7.73 ± 0.04	12.96 ± 0.02
P^+	$^3P_{1\rightarrow0}$	60.640	0.06 ± 0.03	<0.10	0.095 ± 0.025
N^{++}	$^2P_{3/2\rightarrow1/2}$	57.340	0.093 ± 0.033	<0.14	0.25 ± 0.04
O^{++}	$^3P_{2\rightarrow1}$	51.815	0.23 ± 0.06	<0.23	0.75 ± 0.08

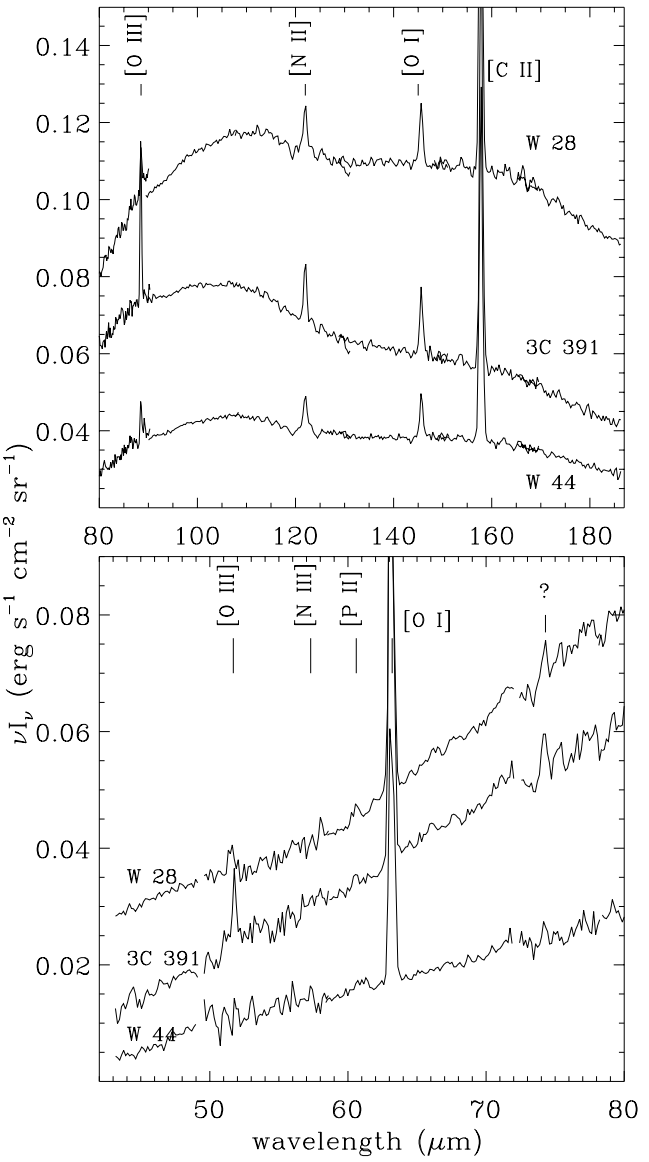

FIG. 1.—*ISO* LWS spectra of molecular shocks in the supernova remnants W28, 3C 391, and W44. The lower and upper panels show the wavelength ranges 42–80 and 80–187 μm, respectively. The ordinate in both panels is νI_ν; to measure line fluxes note that the resolution of the LWS is $\Delta\nu = 0.29$ μm for the top panel and 0.6 μm for the bottom panel. Note that no reference spectrum has been subtracted, so the continuum and [C II] line are partly due to line-of-sight dust and gas. The other bright atomic fine-structure lines are due to the remnants. Some of the minor wiggles at long wavelengths are molecular lines (Reach & Rho 1998), while detector noise is significant at the shortest wavelengths. The unidentified line is labeled with a question mark.

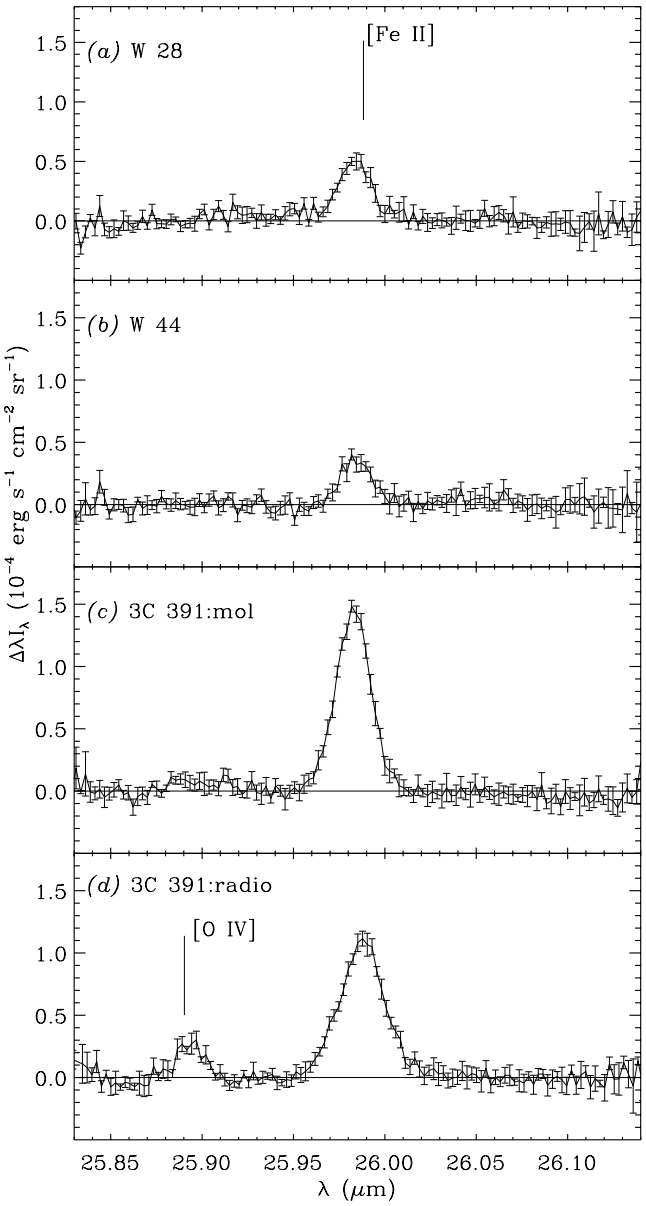

FIG. 2.—*ISO* SWS spectra of the ground-state [Fe II] fine-structure line for lines of sight toward molecular shocks in (*a*) W28, (*b*) W44, and (*c*) 3C 391; also the spectrum for a line of sight toward the radio peak in 3C 391. The molecular shock positions all show bright [Fe II] lines. The radio peak position in 3C 391 also shows a bright ground-state fine-structure line of [O IV]. The solid curves are Gaussian fits to the line with width fixed to the SWS grating spectral resolution of $\Delta\lambda = 0.018$ μm.

TABLE 2

SWS SPECTRAL LINE RESULTS

ION	TRANSITION	WAVELENGTH	LINE BRIGHTNESS (10^{-4} ergs s^{-1}cm^{-2}sr^{-1})			
			W28	W44	3C 391:BML	3C 391:Radio
Fe^{+}	$^6D_{7/2\rightarrow9/2}$	25.988	0.66 ± 0.05	0.41 ± 0.04	1.9 ± 0.1	1.8 ± 0.1
O^{+++}.....	$^2P_{3/2\rightarrow1/2}$	25.890	<0.08	<0.08	<0.08	0.12:
Si^{+}	$^2P_{3/2\rightarrow1/2}$	34.815	7.3 ± 0.1	4.8 ± 0.1	15 ± 0.2	13 ± 0.2
H_2.....	$S(3)$	9.665	10.2 ± 0.1	3.6 ± 0.1	1.95 ± 0.05	0.32 ± 0.06
H_2.....	$S(9)$	4.695	1.2 ± 0.1	1.9 ± 0.1	1.3 ± 0.1	<0.2

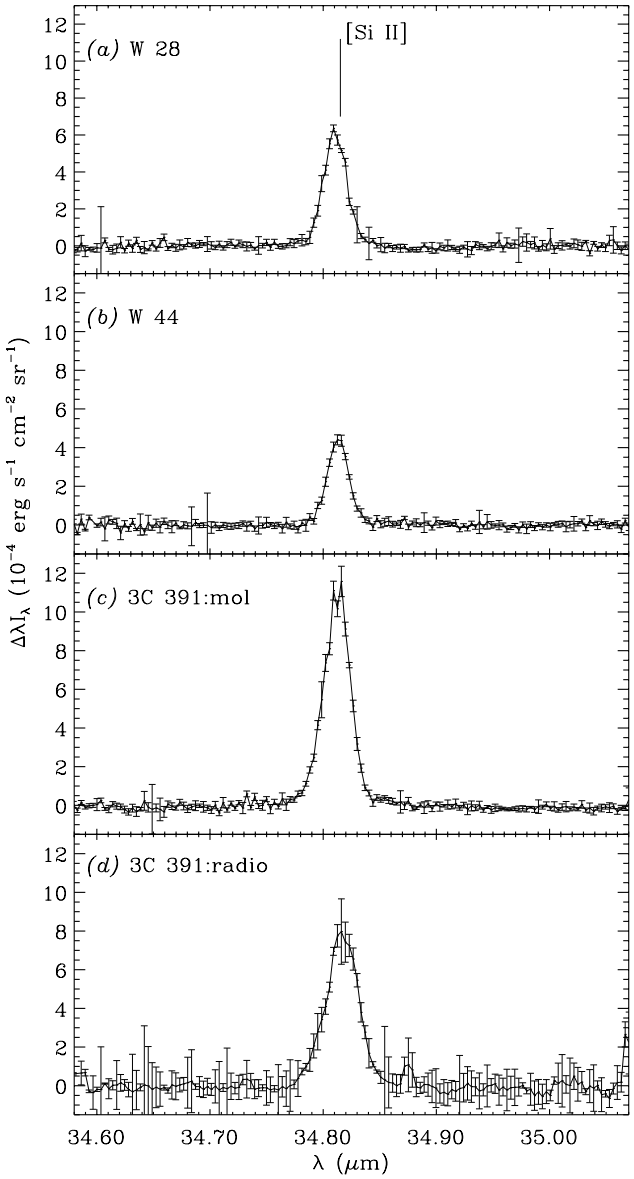

FIG. 3.—*ISO* SWS spectra of the ground-state [Si II] fine-structure line for lines of sight toward molecular shocks in (*a*) W28, (*b*) W44, and (*c*) 3C 391; also the spectrum for a line of sight toward the radio peak in 3C 391. The solid curves are Gaussian fits to the line with width fixed to the SWS grating spectral resolution of $\Delta\lambda = 0.022$ μm.

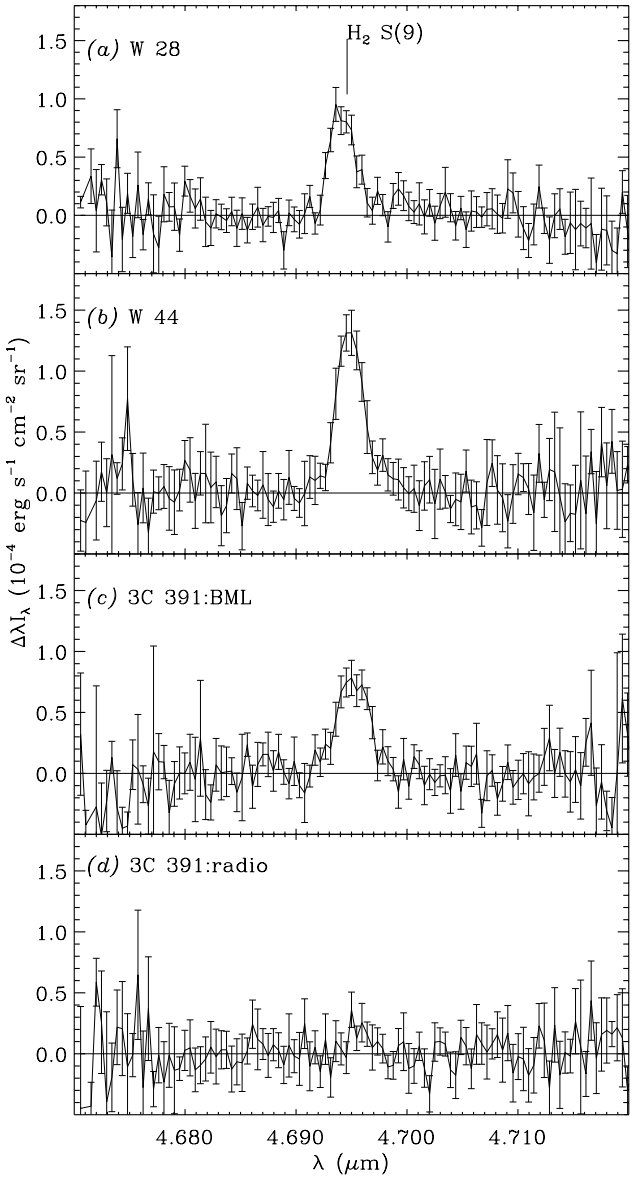

FIG. 4.—*ISO* SWS spectra of the H_2 *S*(9) rotational line toward molecular shocks in (*a*) W28, (*b*) W44, and (*c*) 3C 391; also the spectrum for a line of sight toward the radio peak in 3C 391. The solid curves are Gaussian fits to the line with width fixed to the SWS grating spectral resolution of $\Delta\lambda = 0.0021$ μm.

relative to the ionic lines, is more than a factor of 10 lower for 3C 391:radio than for 3C 391:BML. This is consistent with the millimeter-wave molecular lines revealing no evidence for shocked molecular gas toward 3C 391:radio, while bright and broad shocked molecular lines were detected toward 3C 391:BML (Figs. 2 and 4 of Reach & Rho 1999). The spectra of these two positions serve a valuable comparison and diagnostic tool, because one of them is dominated by ionic lines, while the other has significant molecular emission.

2.3. *High-Resolution* [O I] *and* CO *Spectra*

We used the Fabry-Perot in the LWS to obtain high-resolution spectral profiles of the [O I] 63 μm lines for 3C 391:BML and W44. The positions are the same as those where the complete LWS spectra and the SWS line spectra were taken, and they correspond to peaks in the [O I] strip maps presented in Reach & Rho (1996, hereafter Paper I).[2] The instrumental resolution of the LWS Fabry-Perot is 36 km s^{-1}. The two spectra are shown in Figures 6 and 7. The lines are clearly resolved, with a full width at half maximum (FWHM) of 100 km s^{-1}. The lower panels of Figures 6 and 7 show the CO(2→1) and ^{13}CO(1→0) line profiles for the same lines of sight as the O I spectra, obtained with the IRAM 30 m telescope (Wild 1995). The observing techniques are described in our previous paper, where the 3C 391 observations were presented (Reach & Rho 1999); the W44 observations are new. The line profiles are all

[2] Please note that the apparent 400 km s^{-1} shift in line center in 3C 391 from one side of the remnant to the other, mentioned in Paper I, is apparently an instrumental artifact due to mapping in the dispersion direction of the grating. The observations presented in this paper, with the Fabry-Perot, are considered reliable measurements of the line profile.

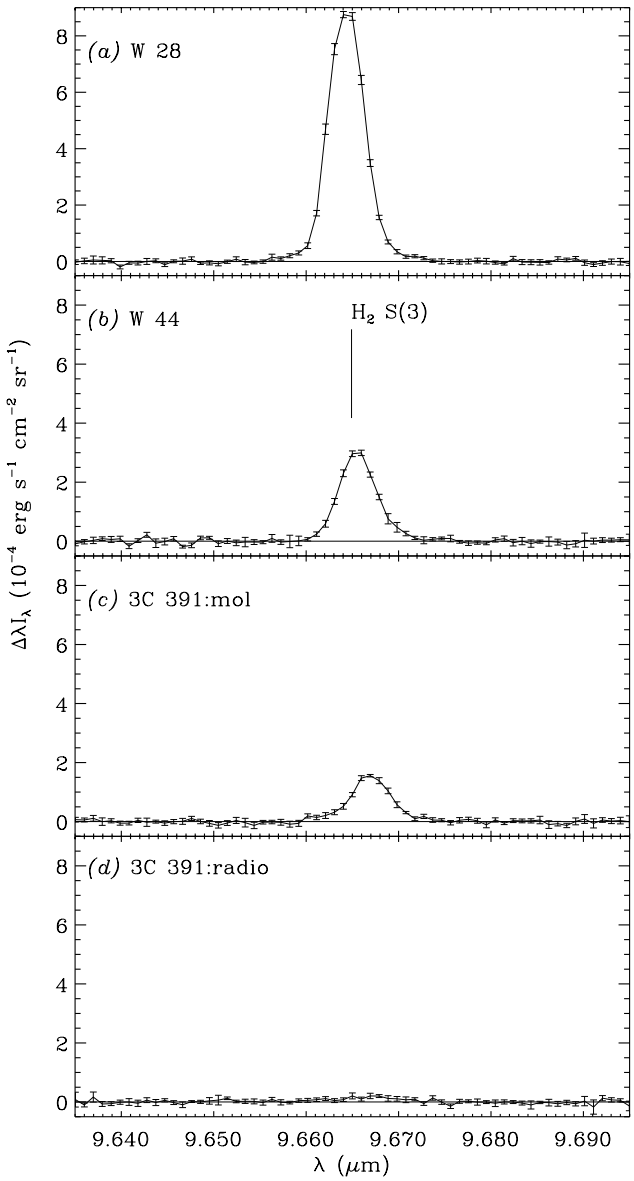

FIG. 5.—*ISO* SWS spectra of the H_2 $S(3)$ rotational line toward molecular shocks in (*a*) W28, (*b*) W44, and (*c*) 3C 391; also the spectrum for a line of sight toward the radio peak in 3C 391. The solid curves are Gaussian fits to the line with width fixed to the SWS grating spectral resolution of $\Delta\lambda = 0.0042$ μm.

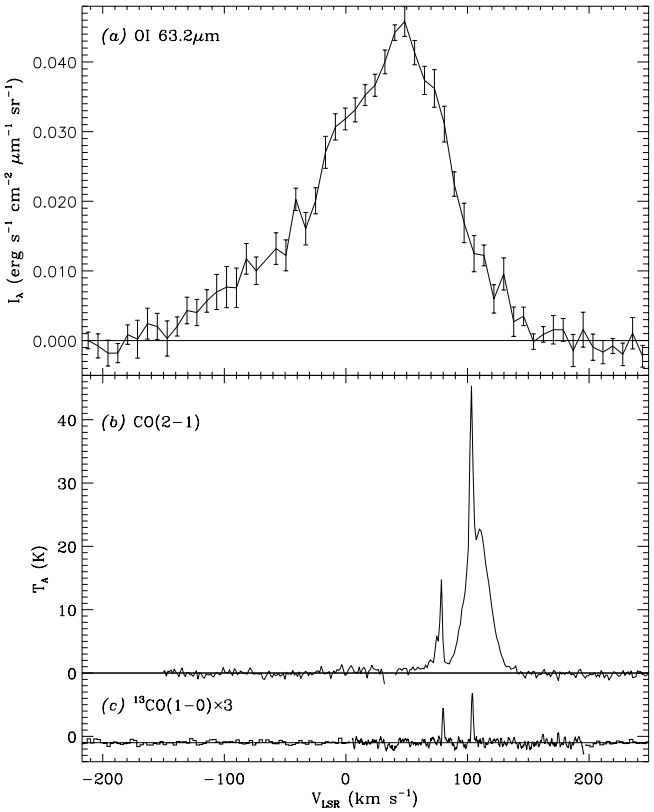

FIG. 6.—(*a*) High-resolution *ISO* LWS spectrum of the O I line toward 3C 391:BML. The instrumental resolution is 36 km s^{-1}, so the line is clearly resolved. (*b*, *c*) Spectra of the CO(2→1) and ^{13}CO(1→0) lines for the same line of sight, obtained with the IRAM 30 m telescope. The ^{13}CO line arises only from unshocked gas, while the CO(2→1) line has a wide component from the shocked gas as well as narrow components from the unshocked gas.

clearly, very different. The ^{13}CO lines have a narrow (1.5 km s^{-1} FWHM) velocity dispersion, and they trace the column density, so they arises from large clouds of cold, unshocked or unrelated gas. Although the CO(2→1) lines also have narrow components, identical to the ^{13}CO lines, from the unshocked or unrelated gas, the CO(2→1) lines are dominated by a broad component (20–50 km s^{-1} FWHM). The broad component was seen in the CO, CS, and HCO^+ observations of 3C 391, with relatively more emission from the higher excitation and higher dipole moment lines (Reach & Rho 1999). Similarly, the CO observations of W28 showed that the broad component was much brighter than the narrow component in the 3→2 line as compared to the 1→0 line (Arikawa et al. 1999). The broad components of the molecular lines are still not as broad as the [O I] line, suggesting that each of the spectral lines in Figures 6 and 7 trace different regions.

Inspecting the [O I] line profiles, there is only slight evidence for structure. The lines from both remnants can be reasonably represented by Gaussians with FWHM ~ 100 km s^{-1}. For 3C 391:BML, the line profile is somewhat better represented by multiple components: an unresolved component centered near 50 km s^{-1} and a broad, non-Gaussian component centered near 0 km s^{-1} with 120–150 km s^{-1}. The integrated line brightness is dominated by the wider component. The unresolved component contributes only about 10% of the line integral, and it may be associated with preshock or unrelated gas, which would agree with the brightness of the "off-remnant" positions from the [O I] strip map (Reach & Rho 1996). Neither 3C 391 nor W44 show evidence for self-absorption in the line profiles. This was a particular concern in interpreting the line brightnesses for molecular supernova remnants, both because of the possibility of dense preshock clouds and the large column densities of cold gas along the lines of sight to the remnants. A single cold cloud might be expected to yield an essentially unresolved (Gaussian) absorption dip, which does not occur. The foreground gas would be expected to absorb in approximate proportion to the line of sight column density. After inspecting the H I 21 cm profile for these lines of sight, we found no correlation that could be due to absorption dips. Instead, it is likely that the line-of-sight gas contributes slightly to the *emission*. The level of [O I] emission from the line-of-sight gas is most easily

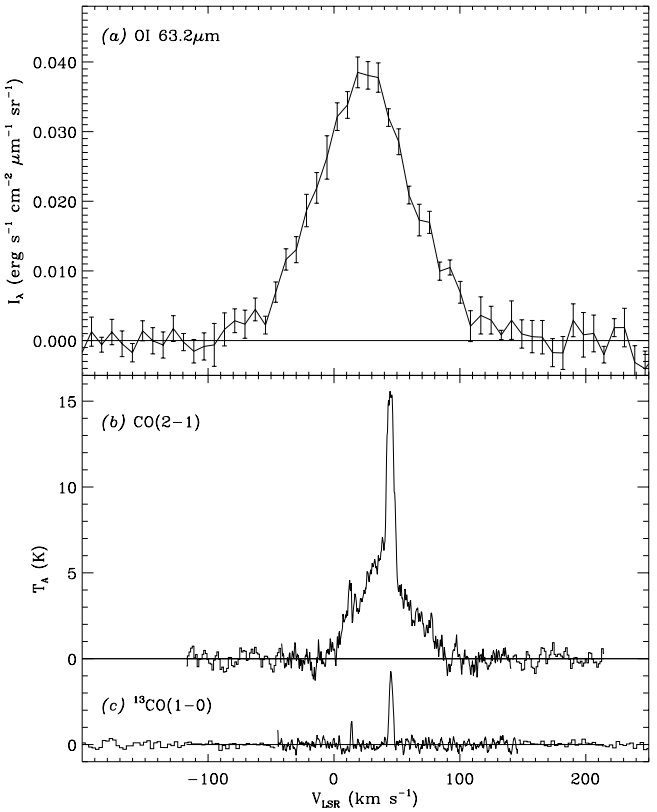

FIG. 7.—(*a*) High-resolution *ISO* LWS spectrum of the O I line toward W44. (*b*, *c*) Spectra of the CO(2→1) and ^{13}CO(1→0) line for the same line of sight, obtained with the IRAM 30 m telescope.

estimated from the reference positions just outside the remnant, where it was found to be quite faint (Reach & Rho 1996). Therefore, we interpret the [O I] line profiles in Figures 6 and 7 as emission from the shocked gas. This inference yields a direct measure of the shock velocity of 100–150 km s^{-1}, albeit in projection along the line of sight. There are likely to be multiple shocks within the beam, and the FWHM of the line profile is approximately equal to the "typical" shock velocity.

Comparing the [O I] and CO line profiles, we can partially describe the three-dimensional geometry of the shocks. For 3C 391, note that the centroids of the [O I] and CO lines are very different. The CO line occurs at nearly the systemic velocity at the remnant's distance, with the broad component due to the shocked gas very slightly blueshifted from the narrow line from the preshock gas. The [O I] line, on the other hand, is significantly redshifted from the preshock gas. Thus, the shock that produces the [O I] line has a significant velocity component toward us; that is, the shock is propagating partially along the line of sight. This suggests that the 3C 391 progenitor exploded on the far side of its parent molecular cloud, driving the dense blast wave partially in our direction. For W44, the centroids of the [O I] and CO lines are similar, suggesting that the shocks are either perpendicular to the line of sight, or that the lines come from similar geometries. One straightforward conclusion from comparing the line profiles, both in centroid and width, is that the [O I] line does not arise exclusively from slow shocks into very dense gas such as produces the CS, OH, and H_2O emission (Reach & Rho 1999). Instead, most of the [O I] emission must arise from faster shocks into moderate-density gas.

3. COMPARISON OF DETECTED LINES TO THE PERIODIC TABLE

3.1. *Atomic Fine-Structure Lines: Basic Principles*

The three basic principles that determine which spectral lines will be bright in the spectrum of a parcel of gas are abundance, ionization, and excitation. The abundances of the elements are given by Anders & Grevesse (1989) for the solar system. In the interstellar medium, since part of the abundance will be locked in solids, the gas phase abundance will be smaller than solar system abundance for some elements (Savage & Sembach 1996). It is clear that we need only consider the top three rows of the periodic table and the middle of the fourth row; all other elements have negligible abundance. The ionization state of each element depends on where the gas is located. We can consider three typical locations: the diffuse interstellar medium (where all electrons bound by less than 13.6 eV are removed), dark clouds (where elements are neutral), and hot plasmas (where the higher ionization states are present). The excitation of the atomic levels will depend on the density and temperature of the region, but a "zeroth" order effect determines whether there are any atomic fine-structure lines in the ground electronic state. Elements and ions with zero angular momentum ($L = 0$) in their ground state electron configuration will not have the fine-structure lines considered here. For example, in spectroscopic notation, S configurations have no lines, while doublet ^{2}P configurations have one line and triplet ^{3}P configurations have two lines. The fine-structure lines are magnetic dipole transitions, so they are technically "forbidden lines," but with spontaneous radiative decay rates of order 10^{-5} s^{-1} and collisional de-excitation rates of order 10^{-7} cm^{-3} s^{-1}, they are easily excited under astronomical conditions and are thermalized at densities $\gtrsim 10^2$ cm^{-3} (for far-infrared lines) to 10^4 cm^{-3} (some mid-infrared lines).

In order to understand and predict which fine-structure lines are present in astronomical spectra, we constructed a "periodic table for astronomical fine structure lines." Table 3 contains the electron configurations and wavelengths for the *p*-shell ions of the second and third rows of the periodic table (C, N, O, Fe, Ne, Al, Si, P, S, Cl, and Ar), while Table 4 has the same information for the fourth row of the periodic table (Cr, Mn, Fe, CO, and Ni). In both tables, the dominant ionization state in the diffuse interstellar medium is shown in boldface. Spectra of regions behind shock fronts or with very high radiation fields will contain the dominant ionization state as well as and the ions to the left of the dominant ionization state. Spectra of regions that are shielded from the interstellar radiation field will contain neutral forms and ions to the right of the dominant ionization state. Some elements with negligible astronomical abundance are not listed; also, to reduce clutter, unlikely ionization states of rare elements are not listed. Alkaline metals (in low-ionization states) have no *p*-shell electrons to make infrared fine-structure lines, so they are not listed. These tables can be used both to predict which lines will be present for a given gas and to decide which lines *should* be present when another line of the same ion is detected. In all cases, the transitions are simple cascades down a ladder, with the ground state at the bottom; therefore, the upper

TABLE 3

"PERIODIC TABLE" FOR ASTRONOMICAL FINE-STRUCTURE LINES: $Z = 6$–18[a]

Element (1)	Abundance[b] (2)	$^2P_{1/2}$ (3)	$^3P_0$ (4)	$^4S_{3/2}$ (5)	$^3P_2$ (6)	$^2P_{3/2}$ (7)	$^1S_{3/2}$ (8)
C	−3.4	**II**$_{157.7}$	I$^{370}_{610}$				
N	−3.9	III$_{57.3}$	II$^{121.9}_{205.9}$	**I**...			
O	−3.1	IV$_{25.9}$	III$^{51.8}_{88.4}$	II...	**I**$^{145.5}_{63.2}$		
F	−7.5				I$^{67.2}_{29.3}$	**I**$_{24.8}$	
Ne.....	−3.9			*IV*...	*III*$^{36.0}_{15.6}$	II$_{12.8}$	**I**...
Al	−5.5	I$_{89.2}$					
Si.....	−4.4	**II**$_{34.8}$	I$^{68.4}_{129.7}$				
P	−6.4	III$_{17.9}$	**II**$^{32.9}_{60.6}$	I...			
S.....	−4.7	IV$_{10.5}$	III$^{18.7}_{33.5}$	**II**...	I$^{56.3}_{25.2}$		
Cl	−6.7			III...	**II**$^{33.3}_{14.4}$	I$_{11.3}$	
Ar	−5.4			IV...	III$^{21.8}_{8.99}$	II$_{6.99}$	**I**...

[a] The headings of cols. (3)–(8) give the spectroscopic notation ^xY_z for the ground state. Roman numerals represent the ionization state (I—neutral; II—singly ionized, ...), with the dominant ionization state in the diffuse interstellar medium in boldface. Small numbers indicate the wavelength of the ground-state fine-structure lines, in μm. The transition to the true ground state is at the bottom and increasing energy levels are above, when applicable. All wavelengths of spectral lines that we detected are shown in italics. Zero-spin ground states, which have no fine-structure lines, have ellipses in their wavelength column.

[b] A is the base-10 logarithm of the abundance relative to H.

energy level for a line can be calculated by summing the photon energies from a given line to the bottom.

3.2. *Comparison of Detected Lines to the Periodic Table*

In the "periodic table for atomic fine-structure lines" (Tables 3 and 4), the lines we detected from molecular supernova remnants observations are in *italics*. It appears that we detect all of the available ground-state fine-structure lines of the astronomically abundant molecules; the undetected ground-state lines are generally outside our wavelength range. All abundant elements, C, N, O and Si, are detected as shown in Tables 1 and 2. Nondetections of F and Co lines are due to low abundances. Lines from high-ionization states were also not detected. The only element with high abundance that we did not detect is Ne, because our observations did not cover the wavelengths of its ground-state fine-structure lines. Our own observations contain the wavelengths of 12 fine-structure transitions among energy levels within 600 K of the ground state, from elements with abundance greater than 10^{-7} relative to H in their expected ionization states. We detect essentially all of these lines, as well as lines from higher ionization states of the abundant elements: O III, O IV, and N III. In addition to these, the ground-state line of [P II] is also detected for W28 and 3C 391. Some of the other lines were detected in the younger and brighter supernova remnant RCW 103 (Oliva et al. 1999b); upon reanalysis of these data from the *ISO* archive, we find that the detected lines include the ground-state line of [P II]. We can use these general principles to predict other bright lines, outside of our observed spectral range. For example, Ne is a very abundant element with lines in the mid-infrared; given that we detected ionized states of O, we expect bright emission from [Ne II] at 12.8 μm and perhaps [Ne III] at 15.5 μm.

TABLE 4

"PERIODIC TABLE" FOR ASTRONOMICAL FINE-STRUCTURE LINES: $Z = 24$–28[a]

		Number of Electrons											
Element	Abundance	23	24		25		26		27		28		
Cr	6.3	**II**^{6}**S$_{5/2}$**...	I^{7}S$_3$...										
Mn	6.5	III^{6}S$_{5/2}$...	**II**^{7}**S$_3$**...		I ^{6}S$_{5/2}$								
Fe	4.5	IV^{6}S$_{5/2}$...	III^{5}D$_4$	105.4 51.7 33.0 22.9	**II**^{6}**D$_{9/2}$**	87.3 51.3 35.3 25.99	I ^{5}D$_4$	111.2 54.3 34.7 24.0					
Co	7.1				III^{4}F$_{9/2}$	24.1 16.4 11.9	**II**^{3}**F$_4$**	15.5 10.5	I^{4}F$_{9/2}$	16.9 12.3			
Ni	5.7						III^{3}F$_4$	11.0 7.34	**II**^{2}**D$_{5/26.64}$**		I^{3}F$_4$ 7.51		11.3

[a] See caption for Table 3.

4. ABUNDANCES OF THE SHOCKED GAS

4.1. *Excitation of Oxygen*

Based on the arrangement of the energy levels of the ground-state atomic fine structure, the ratios the upper and lower [O I] and [O III] lines constrain the density and temperature of the emitting region, independent of the geometry. The upper panel of Figure 8 shows the line ratio predicted for [O I] as a function of the total H density and temperature. At each density and temperature, the level populations were calculated and the emergent intensity predicted using the escape probability (Hollenbach & McKee 1979). The column density, N_H, was adjusted iteratively for each model such that the model predicts the correct brightness of the [O I] 63 μm line. Solid lines show the locus of models that predict the observed line ratios from Table 1. The locus of models for which the path length through the emitting region, $z = N_H/n_H$, is equal to 3 pc (i.e., comparable to the radius of the supernova remnant) is shown as a dashed contour, and the region below this contour is labeled "region to large." Low-temperature and low-density models are not capable of producing the observed line brightness within the confines of the observed region. Another constraint is drawn as a vertical line at $T = 10^4$ K, where the neutral O atom would be collisionally ionized; higher temperature models should therefore be excluded. The lower panel of Figure 8 shows the line ratio predicted for [O III] as a function of density and temperature, with each model normalized to predict the correct brightness of the [O III] 88 μm line. The [O III] and [O I] emitting regions are not necessarily coincident, so we consider the density, temperature, and ionization in the two regions separately. One relative constraint between the two emitting regions is practically guaranteed: the temperature will be at least as high, the density will be at least as low (and the ionization will be at least as high) in the [O III] emitting region as compared to the [O I] emitting region. This rules out the very dense models for the [O III] emitting region, as indicated by the upper dashed curve in the lower panel of Figure 8.

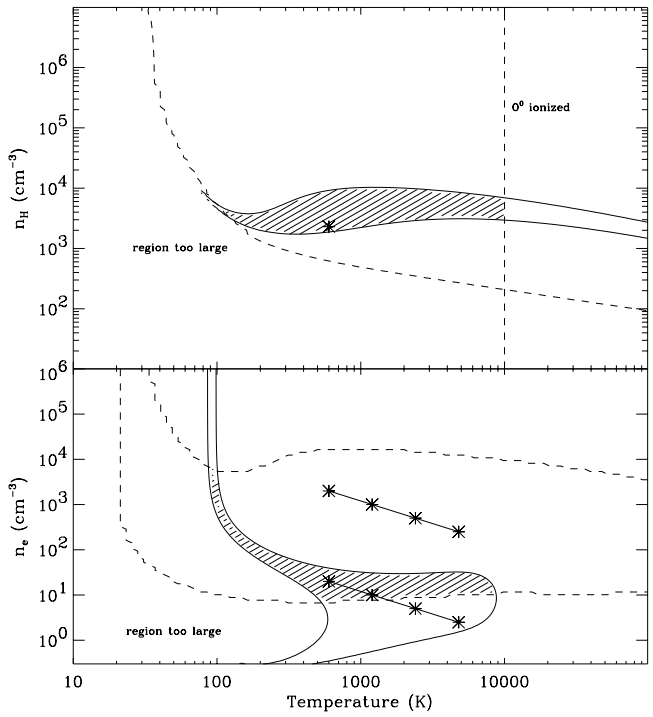

FIG. 8.—Excitation diagrams for the [O I] (*upper panel*) and [O III] (*lower panel*) lines. The solid contours show the observed range of 145/63 μm (*upper panel*) and 52/88 μm (*lower panel*) line ratios from Table 1. The dashed contour running approximately from the upper left to lower right of each panel shows the constraint placed on the density and temperature by requiring that the emitting region is smaller than the entire supernova remnant, while still producing lines as bright as observed. The vertical dashed line in the upper panel at $T = 10^4$ K shows where O should be collisionally ionized. The dashed contour near the top of the lower panel shows the constraint that the O III region be at least as hot and no more dense than the O I region. Hatched regions in both panels show the allowed solutions. The asterisk in the upper panel shows the solution that we chose for detailed calculations. The upper left asterisk in the lower panel shows this same solution if the gas is fully ionized, and the asterisks connect to it show the set of solutions in thermal pressure equilibrium with it. The lower set of asterisks shows the same solutions assuming the ionization fraction in the O III region is 1%.

To determine the physical conditions where the lines are produced, and to determine the abundances of the elements in the shocked gas, we define two emitting regions. Region M (molecular) is the [O I] emitting region, with density, temperature, and column density set to give the observed brightnesses of the 63 and 145 μm lines. Region A (atomic) is the [O III] emitting region, with density, temperature, and column density set to give the observed brightnesses of the 52 and 88 μm lines. Such a separation of emitting regions is anticipated because we expect that the neutral and doubly ionized states of O would not be cospatial—although there could in principle be overlap, if the gas is far from ionization equilibrium. Combining all of the constraints, the plausible range of density and temperature for region M has density $2000 < n_H^{(M)}$ (cm^{-3}) < 5000 and temperature $100 < T^{(M)}$ (K) < 1000 K. For convenience, we have chosen a nominal solution of $n_H^{(M)} = 3000$ cm^{-3} and $T^{(M)} = 600$ K, which is marked with an asterisk (*) in Figure 8 and listed in Table 5, for detailed calculations.

In region A, there is a wider range of solutions within the constraints already mentioned. In particular, models with constant $n_e = n_H x$, where x is the fraction of H that is ionized, produce the same excitation for the ions in region

TABLE 5

PHYSICAL PROPERTIES OF THE THREE POSTSHOCK EMITTING REGIONS

	PRESHOCK		POSTSHOCK			
REGION	n_0 (cm^{-3})	V_s (km s^{-1})	n (cm^{-3})	T (K)	N (cm^{-2})	INFRARED COOLANTS
A (atomic).....	<1	500	8	3000	10^{20}	O III, N III
M (molecular).....	10^2	100	3×10^3	600	10^{21}	O I, Si II, Fe II, N II, H_2 $S(9)$
C (clump).....	10^4	200	4×10^5	20	10^{22}	CO, H_2O, OH, H_2 $S(3)$

A. If region A and region M were layers behind the same shock front, then we expect region A to have a comparable or somewhat higher pressure than region M (lest the shock move backward). For the nominal solution for region M, the region A solutions with the same pressure but density lower by factors of 1, 2, 4, and 8 are shown as two lines connecting asterisks in the lower panel of Figure 8. The upper line applies if region A is completely ionized, and the upper left asterisk is just a direct copy of the region M solution. It is evident that region A cannot be completely ionized *and* be a shock layer upstream from region M: the region A pressure would be so low that the shock would move backward. The lower line applies if region A has an ionization fraction $x = 10^{-2}$, and the upper left asterisk of the lower line is the region M solution with $n_e = n_H/100$. This would be a very surprising result, because it means that O^{++} coexists with a significant amount of H^0. Very low-density gas can be far from ionization equilibrium, with higher ionization states coexisting with neutral states (Schmutzler & Tscharnuter 1993), but at the high densities required to get the observed brightness of the 63 and 88 μm lines the ionization should be reasonably close to equilibrium. For this reason, we consider the [O III] emitting region (region A) separate from the [O I] emitting region. For detailed calculations, the region A model has density $n_e^{(A)} = 8$ cm^{-3} and temperature $T^{(A)} = 3000$ K; the properties are listed in Table 5. In region A, the abundance of O^0 is set to zero, and the abundance of O^{++} and N^{++} are set to the entire cosmic abundance of O and N, respectively.

4.2. *Predicted Line Brightnesses for Different Regions*

The impact of a supernova blast wave with a molecular cloud leads to a complex interaction, with regions of different density reacting in very different ways. Based on the excitation of [O I] and [O III] (discussed in the previous section), and the excitation of H_2O and OH (Reach & Rho 1998), we identify three types of postshock gas and their infrared emitting lines. Figure 9 is a cartoon showing these shocks, and Table 5 lists their properties. The lowest-density preshock gas is region A (for "atomic") with preshock density $n_0^{(A)} < 1$ cm^{-3}. (If the preshock density of region A were higher than 1 cm^{-3}, the postshock density would be much higher than the 8 cm^{-3} and would be inconsistent with the 52/88 μm line ratio.) The postshock gas in region A gives rise to bright H II recombination lines and infrared and optical O III and N III (and other high ion) forbidden lines. The moderate-density preshock gas is region M (for "molecular") with preshock density $n_0^{(M)} \sim 10^2$ cm^{-3}. The postshock gas in region M gives rise to bright O I and most of the other bright infrared forbidden lines we observed, as well as some optical emission (which is, however, highly obscured). The highest-density preshock gas is in the dense clumps, with preshock density $n_0^{(C)} \sim 10^4$ cm^{-3}. The postshock gas in region C gives rise to bright H_2, OH, CO, CS, and H_2O emission, with a possible contribution to the O I emission. We do not mean to imply that there are three sharply defined regions with fixed densities; we do suggest that the full range of preshock densities is needed, such that no single region is consistent with all of the observed spectral lines.

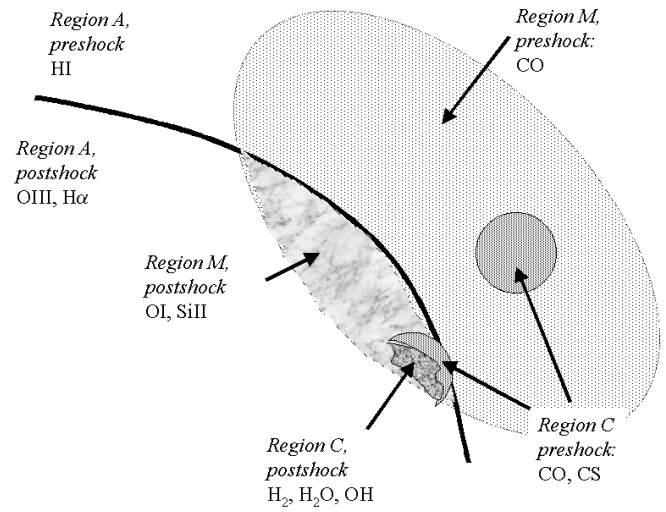

FIG. 9.—Cartoon illustrating the different pre- and postshock regions discussed in the paper. The physical properties of the regions are listed in Table 5. For each region, we also list an ion or molecule whose emission can be used to image the region.

The shock velocities in the different regions are not well known, but reasonable estimates can be made. If region A is the lowest-density preshock gas, then it should represent the leading edge of the supernova remnant. The Sedov solutions for these remnants are consistent with the density of region A for explosions with energy of order 10^{51} ergs (Rho 1995). Thus, the shock velocity should be of order $2R/5t$, where R is the radius and t is the age of the remnant. This works out to $V_s^{(A)} \simeq 500$–600 km s^{-1} for the remnants considered in this paper (Rho 1995; Rho & Petre 1998). For region M, we have some direct evidence of the shock velocity from the width of the O I line (§ 2.3) that $V_s^{(M)} \simeq 100$ km s^{-1}. This is also consistent with the expanding H I shell observed toward W44 (Koo & Heiles 1995). For region C, there is some direct evidence of the shock velocity from the width of the millimeter-wave CO and CS lines (Reach & Rho 1999) that $V_s^{(C)} \simeq 30$ km s^{-1}. The shock ram pressure $p_{ram} \propto n_0 V_s^2$ should be comparable in these regions as they are all driven by the same blast wave. Indeed, we find p_{ram} is progressively higher for the denser regions, but the range of p_{ram} is only a factor of 36. A pressure enhancement in the denser regions has been theoretically justified by Chevalier (1999) as due to the shock into the denser gas (regions M and C) being driven from the radiative shell (region A) as opposed to being isolated shocks driven by the blast wave.

In Chevalier's (1999) paper, two regimes of density were considered for the preshock gas; these densities correspond roughly to our regions A and M (cf. Table 5). Chevalier explained the [O I] 63 μm luminosity of the remnant using only relatively low-density shocks into region A. Based on our new results for the line ratio and excitation of O I and the high-resolution spectrum of the 63 μm line showing a width of only 100 km s^{-1}, we suspect that the 63 μm arises in relatively denser regions, like region M. Indeed, it is impossible for a low-density emitting region to produce 63 μm lines as bright as we observed, within the confines of the supernova remnant. In the model of Hollenbach & McKee (1989), the 63 μm line brightness is proportional to $n_0 V_s$. For the cartoon model parameters in Table 5, it is clear that the denser regions will dominate the line brightness if they fill an appreciable portion of the beam. In region C, however, the O is probably largely tied up in molecular form; furthermore, region C is somewhat beam diluted in

TABLE 6

MODEL PREDICTIONS FOR FINE-STRUCTURE LINES

Ion	Abundance	Line Wavelength (μm)	Atomic Data References[a]	Observed (ergs cm^{-2} s^{-1} sr^{-1})	Observed/Predicted	
					Layer M[b]	Layer A[c]
C II.....	−3.44	157.7	1	5.8×10^{-4}	1.2	...
N II	−3.95	121.9	1	2.7×10^{-4}	0.3	10
N III.....	−3.95	57.3	2,3	9.7×10^{-3}	...	0.3
O I	−3.07	63.2	4,5	1.3×10^{-3}	1.0	...
O I	−3.07	145.5	4,5	9.1×10^{-5}	1.0	...
O III.....	−3.07	88.4	1	5.2×10^{-3}	...	1.0
O III.....	−3.07	51.8	1	2.8×10^{-3}	...	0.9
Si II	−4.45	34.8	5	3.0×10^{-3}	0.5	10
P II.....	−6.55	60.6	6,7	8.6×10^{-6}	1.1	...
Fe II.....	−4.33	26.0	8	2.7×10^{-4}	0.3	10

[a] References for atomic data. (1) Spitzer 1978; (2) Froese Fischer 1983; (3) Blum & Pradhan 1992; (4) Launay & Roueff 1977; (5) Hollenbach & McKee 1989; (6) Mendoza & Zeippen 1982; (7) Kreuger & Czyzak 1970; (8) Nussbaumer & Storey 1982.

[b] Layer M model parameters: $n = 3000$ cm^{-3}, $T = 600$ K, O III and N III abundances set to zero, column density normalized to produce observed [O I] lines.

[c] Layer A model parameters: $n_e = 8$ cm^{-3}, $T = 3000$ K, O I abundance set to zero, column density normalized to produce observed [O III] lines.

the *ISO* LWS beam. Therefore, we believe that the 63 μm lines presented here arise from shocks into the moderate-density molecular gas of region M.

For regions A and M, we calculated the model brightness of all of the lines that we observed with *ISO*. Each element was assumed to have its entire solar abundance in the gas phase and in the ionization state that gives rise to the line, with the following exceptions. In region M, oxygen was assumed to be neutral (as we observed), and nitrogen was assumed to be singly ionized (since the only detected line was from N II, not N I) in order to obtain an upper limit to the predicted N II brightness. In region A, oxygen was assumed to be ionized. Our purpose in these calculations is to measure the richness or depletion relative to solar abundances. Our calculations do not yield absolute abundances, because in reality the total abundance of each element is actually divided among the ionization states that are present. In the next section, we go through the list of elements and discuss their expected ionization state and the inferred total abundances in the postshock gas. Table 6 shows the brightness predictions for regions A and M. We can conclude the following, without considering the ionization balance. First, it is possible to reproduce all of the observed fine-structure lines, except N III and O III using region M alone. (In fact, it is possible to get the N III and O III lines, if we could accept the multiply ionized species existing in region M, where H is mostly neutral.) Therefore, we expect to be able to derive abundances in the "region M" postshock gas. For region C, we discuss details in § 5 below.

4.3. *Postshock Gas Abundances*

We now step through each element and derive the total abundance of that element in the postshock gas. Table 7 summarizes the abundances inferred for the postshock gas. For each element X, $[X/H]_\odot$ is the solar abundance (Anders & Grevesse 1989) and $[X/H]_{obs}$ is the total abundance of that element from our observations and model.

Carbon.—The only carbon line we observed was from C II, which is likely to be the dominant ionization state in region M. The observed line brightness compared to the region M prediction (Table 6) requires essentially all of the carbon to be in the gas phase. However, a significant fraction of the 157 μm line could come from line-of-sight gas, so this result is inconclusive. The carbon abundance in the postshock gas could be better addressed if we knew the brightness of the line just outside of the remnant. Using our current knowledge, we can only say that the *ISO* observations are consistent with complete destruction of the C-bearing dust grains if all of the emission comes from the remnant, or partial or no destruction if less than half of the emission comes from the remnant. In Table 7 we list the inferred depletion of carbon in the postshock gas assuming *all* of the 157 μm line comes from the remnant; this yields an upper limit to the gas-phase abundance, and therefore lower limit to the depletion.

Nitrogen.—We observed nitrogen in its singly and doubly ionized states. The dominant state in region M should be neutral, because the ionization potential of N I is greater than 13.6 eV. Comparing the observed to predicted brightness (Table 6), we require only about $\frac{1}{3}$ of the nitrogen to be N II, which is reasonable. When all nitrogen is assumed to be singly ionized, the observed to predicted brightness ratio of [N II] is only 0.3 (Table 6), which implies either nitrogen has lower abundance or the predicted N II is too high. Since the former is unlikely, the ratio implies that only about $\frac{1}{3}$ of the nitrogen is N II and the rest is neutral. In region A, which was normalized to give the correct 88 μm

TABLE 7

ABUNDANCES

Element	$\log [X/H]_\odot$	$[X/H]_{obs}/[X/H]_\odot$
C	−3.44	<1.1
N.....	−3.95	>0.3[a]
O.....	−3.07	1
Si.....	−4.45	0.5
P	−6.55	1.1
Fe	−4.33	0.3

[a] Abundance of N is a lower limit because the dominant ionization state (N I) was not observed.

line brightness, we require about $\frac{1}{3}$ of the N III, which is also plausible. In Table 7 we list the depletion of nitrogen assuming all of the nitrogen is ionized; this is a lower limit to the gas-phase abundance, and an upper limit to the depletion, because it neglects the neutral state.

Oxygen.—The column density of our model was adjusted to match the observed brightness of the oxygen lines, so most of our measurements are, effectively, relative to the O abundance. We cannot easily determine the total abundance of O because we lack an accurate measurement of the total column density of H.

Silicon and iron.—We find that a significant fraction of the total abundance of Si and Fe, which are normally highly depleted into dust grains in the interstellar medium, is required to produce the observed line brightness. Both Si and Fe were observed in their dominant ionization state in region M. Region A does not have enough column density to contribute significantly to the observed line brightness. (Recall that the region A column density is set by the [O III] line brightness, so increasing its column density would make too much [O III] emission.) For region M, we find that about $\frac{1}{2}$ of the Si and $\frac{1}{4}$ of the Fe are required to be in the gas phase. These abundances of Fe and Si are interestingly comparable to those of gas-phase abundances in intermediate-velocity interstellar clouds which are recently measured using Goddard High Resolution Spectrograph, suggesting that resilient cores of grains are not easily destroyed in shocks (Fitzpatrick 1996). We will discuss the implications for grain destruction more in § 6.2 below.

Phosphorus.—The abundance of P is known for only a few lines of sight in the interstellar medium. Our abundance estimate in the postshock gas uses the observed brightness of the 60.6 μm line, for which this is the first reported detection (at the time of writing). Figure 10 shows the spectrum of this newly detected line. We used the radiative decay rates are as given by Mendoza & Zeippen (1982), and we use the collision strength $\Omega(^3P_1 \rightarrow 0) = 1.46$ (Krueger & Czyzak 1970). The P abundance relative to O is very well constrained because the energy levels of the two observed ions are similar, and both elements were observed in their dominant ionization state. We find that the observed line brightness is consistent with solar abundance of P. Along the line of sight toward ζ Oph, it appears that about half of interstellar P is normally locked in grains (Savage & Sembach 1996). Our observation suggests that some or all of the P-bearing solid material was vaporized by the strong shock wave, as we find for Fe and Si (see § 6.2).

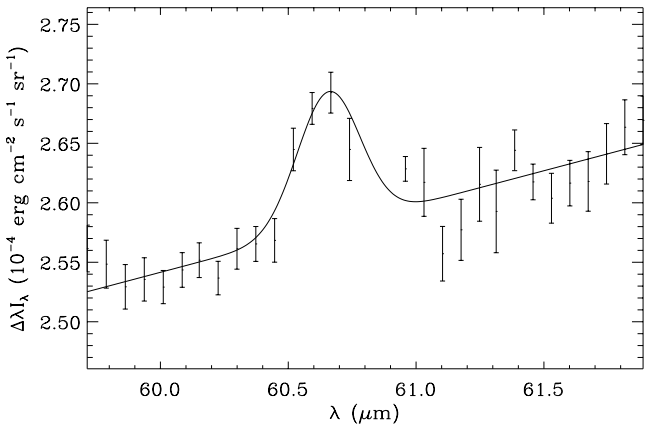

FIG. 10.—Spectrum of the P II 60.6 μm line toward 3C 391:BML. The solid curve is a Gaussian fit to the line with width fixed to the LWS grating spectral resolution of $\Delta\lambda = 0.29$ μm.

5. SHOCK-EXCITED MOLECULES

5.1. H_2

The $S(3)$ and $S(9)$ lines of H_2 were both detected from each of the supernova remnants we observed, and the line brightnesses are listed in Table 2. These H_2 lines arise from shocks in the molecular gas, like the CO, OH, and H_2O lines (Reach & Rho 1998). Using our cartoon model, we can now localize which region(s) give rise to which lines and further constrain the properties of the dense clumps (region C). First, for region M, if we assume that the H_2 rotational lines are collisionally excited with rotational excitation temperature equal to the kinetic temperature, we predict that the brightest H_2 line is the $S(3)$ line. The brightness of the $S(3)$ line from region M, assuming all of the H is in H_2, is 2×10^{-4} ergs cm^{-2} s^{-1} sr^{-1}. This is in very good agreement with the observed line brightness, suggesting that the H is largely molecular behind the region M shocks. The column density of H_2 is just enough that H_2 molecules are self-shielded from dissociating photons in the interstellar radiation field (Hollenbach, Werner, & Salpeter 1971).

We cannot explain the brightness of the higher H_2 $S(9)$ rotational line, or the higher lying ro-vibrational lines in the near-infrared, using the region M shocks. These lines most likely arise in molecular regions that are much warmer than the recombined molecules behind a fast, dissociative shock. Instead, the $S(3)$ lines probably arise from nondissociative shocks into denser gas (discussed below).

In a previous paper (Reach & Rho 1998), we derived the physical properties of region C using the excitation of CO, OH, and H_2O. In that paper, we found the puzzling result that abundance of H_2O was lower than expected in a region with "warm" chemistry, where O is efficiently converted into molecules and OH is converted into H_2O. Two papers have shown that OH can be formed from dissociation of H_2O (Lockett et al. 1999; Wardle 1999), so the abundance OH is no longer such a puzzle. We now reexamine the H_2O abundance relative to H_2. The column density of H_2O was found to be $\sim 3 \times 10^{17}$ cm^{-2} using the far-infrared line brightnesses. The column density of H_2 was taken from the volume density times path length, yielding $\sim 8 \times 10^{23}$ cm^{-2}. We suggested this column density was consistent with the brightness of the H_2 $S(3)$ line, but we now suspect that much of the $S(3)$ line arises from region M and not the dense shock of region C. If this is true, then the H_2 column density of region C could be much lower than we estimated before. Let us start with some assumptions about the molecular abundances and infer the H_2 abundance. First, CO:OH:H_2O is 100:1:15 from our observations (Reach & Rho 1998). Assume that the C and O are largely in molecules. If a fraction f_{CO} of the C is locked in CO, then the abundance ratio of H_2O/H_2 is $X_O f_{CO}$, where X_O is the abundance of O. The column density of H_2 is then $N(H_2)^{(C)} = 3 \times 10^{21} f_{CO}^{-1}$. Such a column density for region C seems reasonable, but it is lower than our previous estimate based on the observed size of the CO emitting region in the millimeter observations (Reach & Rho 1999). This could be explained by a low filling factor for the dense gas, of order $0.007 f_{CO}^{-1}$ in the *ISO* SWS beam. Taking $f_{CO} = 0.5$ as an example, the size of the emitting region would be of order 1″, and it would be highly structured in future, higher

angular-resolution observations. If true, this new interpretation would change our estimate of the mass of the 3C 391:BML postshock gas, making the self-gravity of the shocked gas negligible, and weakening our argument that the dense clump might imminently collapse to form stars (Reach & Rho 1999). Table 5 shows the cartoon model for region C assuming $f_{CO} = 0.5$.

The H_2 0–0 $S(9)$ line cannot be assigned to any of the emitting regions that we have defined so far. Its energy level is too high above the ground state to be excited in the cooling region where the far-infrared lines are produced. It is unlikely that the $S(9)$ line can be produced in the region M shock, even upstream from the cooling region, because the H_2 is probably still dissociated. Thus, we suspect that the $S(9)$ line is produced upstream from the region C shock. To get the observed line $S(9)$ brightness, in an emitting region with rotational excitation temperature of order 1500 K, a column density of order 10^{19} cm^{-2} is needed, which could easily fit in the upstream region considering the cooling region has a column density 600 times larger. The 1500 K excitation temperature seems high, but high excitation is predicted by shock models (Draine, Roberge, & Dalgarno 1983) and is required to explain observed line ratios in IC 443 (Rho et al. 2000; Richter, Graham, & Wright 1995). Future observations should be able to distinguish which shocks produce the $S(3)$ and $S(9)$ lines, by measuring the *width* of the lines. According to our cartoon model, much of the $S(3)$ line comes from region M and would have a width of 100 km s^{-1}. The $S(9)$ line comes upstream from region C and would have a width of 30 km s^{-1}. The line profiles of progressively higher excitation lines would evolve from wide to narrow lines.

5.2. *Unidentified Line at* 74.3 μm

One relatively bright line remains unidentified. Figure 11 shows the spectrum of the 74.3 μm line for 3C 391:BML. The line was present in our complete LWS spectra of W28, W44, and 3C 391, and it has also been seen in the remnant RCW 103 (Oliva et al. 1999b) and the planetary nebula NGC 7027 (Liu et al. 1996). Table 8 lists the brightnesses and central line wavelengths for our remnants. The wavelengths are all consistent with 74.26 μm. All of the spectra that contain this line contain also contain both atomic fine-structure and molecular lines. Based on our list of plausible

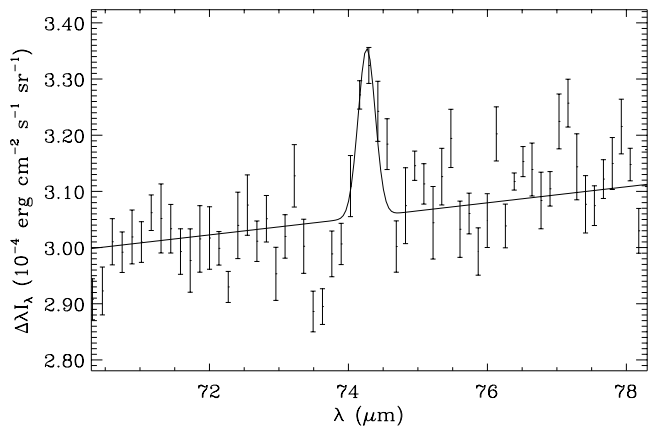

FIG. 11.—Spectrum of an unidentified line toward 3C 391:BML. The solid curve is a Gaussian fit to the line with width fixed to the LWS grating spectral resolution of $\Delta\lambda = 0.29$ μm.

TABLE 8

UNIDENTIFIED LINE

Source	Wavelength (μm)	Line Brightness (10^{-4} ergs s^{-1} cm^{-2} sr^{-1})
3C 391:BML.....	74.26 ± 0.03	0.31 ± 0.05
W44.....	74.32 ± 0.06	0.11 ± 0.03
W28.....	74.25 ± 0.03	0.26 ± 0.04

lines compiled above in Tables 3 and 4, and a careful inspection of all atomic fine-structure lines, we can find no candidate atomic or ionic source for the line. (The only fine-structure line that matches the observed wavelength is a transition among high energy levels of [Ti III], which is extremely unlikely based both on abundance and energetics.) Therefore, we suspect this line is molecular in origin. Despite searching the JPL spectral line database (Pickett et al. 1996), we cannot identify the origin of this line, which is apparently caused by an unusual molecule or metastable state not yet found in laboratories or planetary atmospheres.

6. CONTINUUM AND GRAIN DESTRUCTION

6.1. *Continuum Spectrum*

The moderate-resolution far-infrared spectra are dominated by a bright continuum underlying the spectral lines. Because the remnants we discuss here are in the Galactic plane, much of this continuum emission is likely to be unrelated to the remnant, produced instead by clouds along the line of sight both in front of and behind the remnant, as well as the molecular cloud close to the remnant. We have attempted to extract the remnant contribution to the continuum emission by searching for distinct spatial and spectral variations. In this paper we present a spectral separation of the remnant emission from the unrelated emission; in Paper I and in future work, we use the reference positions and spatial correlations with the O I line brightness.[3]

The continuum spectrum of 3C 391:BML is shown in Figure 12. Even by inspection, it is evident that the spectrum cannot be fitted with a modified blackbody: there is a significant positive excess at wavelengths shorter than 120 μm. It is not surprising for the continuum spectrum to require multiple components. In the *COBE* FIRAS observations of the Galactic plane in a 7° beam, the spectrum of the inner galaxy at wavelengths of 100–200 μm has contributions from two components: 20 K dust associated with atomic gas, and 13 K dust associated with molecular gas (Reach et al. 1995; Lagache et al. 1998). At wavelengths shorter than 100 μm, continuing all the way to the PAH features in the mid-infrared, emission from small, transiently heated dust grains becomes important (Désert, Boulanger, & Puget 1990). For our supernova remnant observations in an 80″ beam, we expect all components to be brighter than in the *COBE*/FIRAS data, because (1) the atomic gas column density peaks sharply in the Galactic

[3] We would like to clarify an issue from Paper I. Despite a statement by Oliva et al. (1999a) that our continuum for W44 is 10 times too bright compared to *IRAS* data, the continuum brightness of the remnant as observed with *ISO* appears real. The *IRAS* data suffer from lower angular resolution, which makes it extremely difficult to separate the remnant from unrelated Galactic emission. The continuum emission will be discussed in more detail in a forthcoming paper.

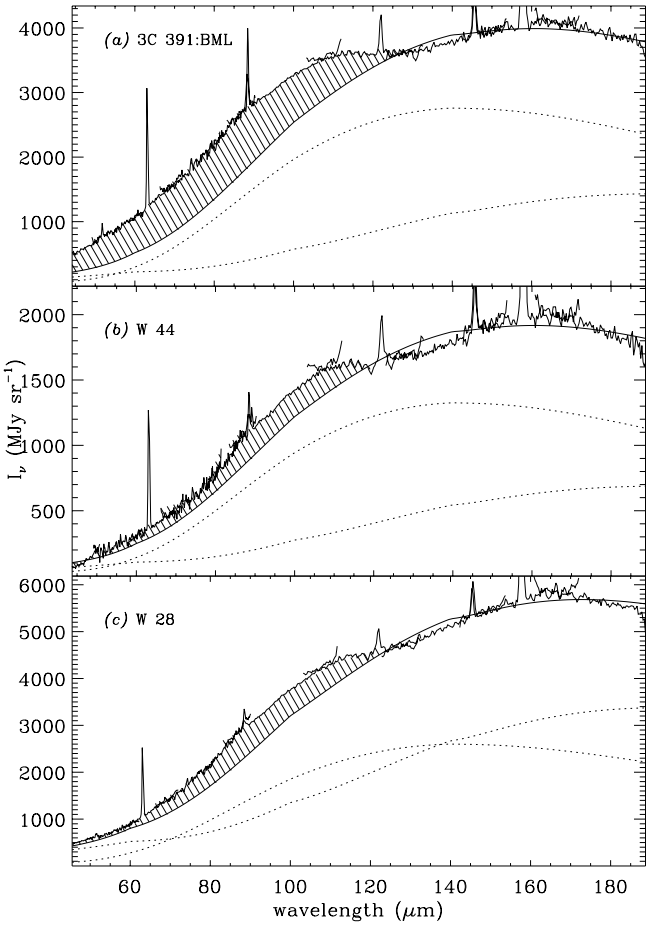

FIG. 12.—Far-infrared continuum spectra toward molecular shocks in (*a*) W28, (*b*) W44, and (*c*) 3C 391. The jagged curve shows the observed brightness. The solid curve shows the spectral model for unrelated dust along the line of sight. This model consists of two components of dust associated with atomic gas ($T_d \sim 20$ K) and molecular gas $T_d \sim 13$ K); each component is shown as a dotted curve. The hatched region shows the excess emission that could be the continuum emission from the remnants. The two dotted curves show the individual contributions of unrelated atomic and molecular gas.

plane, (2) the lines of sight pass directly through giant molecular clouds, and (3) the emission from the remnants themselves are completely beam diluted in the *COBE* FIRAS beam.

To estimate the remnant contribution to the spectrum, we used a nominal spectrum for dust in the local interstellar medium, which big grains, at a temperature of 17.5 K, and small grains with a brightness that matches the *COBE* Diffuse Infrared Background Experiment (Reach & Boulanger 1998 and references therein). We use two components, for the atomic and molecular gas, with radiation fields equal to χ times the local interstellar radiation field. For each component, the temperature of big grains scales as $\chi^{1/6}$, and the brightness of the small grain emission scales as χ. The atomic regions were assumed to have $\chi = 2$ (to account for the enhanced radiation field in the inner Galaxy), and the molecular regions were assumed to have $\chi = 0.5$ (to account for extinction of the ultraviolet radiation field inside molecular clouds). The scale of the model and the ratio of the two components was set to match the far-infrared spectrum at wavelengths longward of 120 μm.

The continuum spectral models are shown for each remnant in Figure 12. The models with a single diffuse ISM component cannot explain the brightness of the continuum at wavelengths shortward of 110 μm; there is a clear excess at 40–110 μm. The amount of excess emission depends rather sensitively on the assumed spectrum of the unrelated interstellar material, so the present results must be used with caution. There is a good correlation of the 74 μm continuum with the O I line brightness (Paper I), supporting our claim that a significant portion of the 40–110 μm emission is from the remnants. There is also a tentative detection of 3C 391 at 60 μm using *IRAS* data (Arendt 1996). This excess emission has a color temperature of $\sim$40 K, corresponding to an enhancement of the radiation field by more than 2 orders of magnitude. Such a high radiation does not occur in the diffuse interstellar medium over many-parsec scales such as observed here. Instead, we must be seeing dust that is either physically different from that in the diffuse interstellar medium, or dust that is excited locally, for example behind the shock fronts. The optical depth of the remnant emission at 100 μm is $\tau \sim 2 \times 10^{-4}$, and the total surface brightness of the far-infrared continuum, assuming a $\nu^2 B_\nu$(42 K) spectrum, is 2×10^{-2} ergs s^{-1} cm^{-2} sr^{-1}. Thus, the infrared continuum is significantly brighter than any of the individual spectral lines. The luminosity of the excess emission, within the single LWS beam that we observed for each remnant, ranges from $\sim$600 $L_\odot$ for 3C 391:BML to $\sim$10 $L_\odot$ for W44 and W28; however, these numbers are rather uncertain. Using the optical depth required to produce the excess emission, the opacity per unit mass for "normal" interstellar dust (Draine & Lee 1985), the mass of shock-excited dust within the single LWS beam that we observed for 3C 391:BML, is $\sim$1 $M_\odot$.

6.2. *Grain Destruction*

In order for the Fe and Si emission lines to be as bright as observed, at least part of the refractory dust mass must have been vaporized. In the cool diffuse cloud toward ζ Oph, 95% of Si and more than 99% of Fe are locked in dust grains (Savage & Sembach 1996). Using our single-slab model, we found that 50% of the Si and 30% of the Fe are required to be in the postshock *gas*, which would mean that about half of the dust mass is destroyed by the shock. The single-slab model will, however, give less accurate measures of the abundances for Fe and Si relative to O (for which the model parameters were determined), because the Fe and Si lines we observed are from higher energy levels than those of O. There is likely to be a stratified postshock emitting region, with somewhat warmer regions producing some of the Si and Fe lines. Thus, the exact fraction of refractory dust mass that was vaporized is highly uncertain. We have experimented with a multiple-slab model, using the approximate density and temperature profiles behind a 100 km s^{-1} J-shock into 10^3 cm^{-3} gas (Hollenbach & McKee 1989), to see how much of the observed 35.2 and 26 μm line brightnesses could be produced by warmer layers closer to the shock. The multiple slab model predicts relatively brighter 26 μm lines for a given column density, by up to a factor of 2 in extreme cases. Thus, it is possible that the gas-phase abundance of Fe was overestimated by up to a factor of 2 using the single-slab model, meaning that as little as 15% of the Fe is required to produce the observed lines. An identical result is obtained for Si. Even with the lower gas-phase abundance of Si and Fe, we can conclude that a nontrivial fraction of the Fe-bearing dust mass was vaporized. It is essentially impossible to produce all of the observed bright-

ness of the 26 μm line from normally depleted preshock interstellar matter.

Using the observed traces of the vaporized and surviving dust grains, we can work backward to estimate the fraction of dust that was destroyed. The total mass of Si and Fe vapor in 3C 391:BML is about 0.11 $M_\odot$, within the LWS beam. Based on the dust-phase elemental abundances in a cold interstellar cloud, the total mass of elements (mainly O, Fe, C, Si, and Mg) in dust is 3.6–5.0 times the mass of Si and Fe in dust, with the lower number coming from B-star reference abundances and the higher number coming from Solar reference abundances (Savage & Sembach 1996). Therefore, we infer that about 0.5 $M_\odot$ of dust was vaporized by shocks into 3C 391:BML. For comparison, our far-infrared continuum observations indicated at least 1 $M_\odot$ of dust remaining in solid form after the shock. Therefore, we estimate that approximately 1/3 of the dust mass was vaporized by the shocks.

How does our inferred fraction of dust vaporization compare to theoretical predictions? Jones, Tielens, & Hollenbach (1996) have calculated the destruction probabilities for dust grains in shock fronts with a range of shock velocities and preshock densities. Their models included sputtering and shattering: sputtering removes material from the grain via collisions with the hot gas, while shattering destroys large grains and creates small grains from them. The models for $v_s = 100$ km s^{-1} are most relevant for the shocks we discuss in this paper. Clearly there are faster shocks that create the X-ray–emitting plasma, and slower shocks that create the molecular line emission. But the ionic lines from which we determined the abundances arise from a layer with a postshock density of order 10^3 cm^{-3} (§ 4) into which shocks with a velocity of about 100 km s^{-1} have been driven (§ 2.3). The model of Jones et al. (1996) with parameters most similar to our present case has preshock density $n_0 = 25$ cm^{-3}. While their models do not extend to higher n_0, the dependence on n_0 is surprisingly mild, with a slight trend toward *more* dust destruction for denser shocks. The models of Jones et al. (1996) predict that about 37% of silicate dust and 12% of graphite dust are destroyed, mostly via nonthermal sputtering. These predictions are in excellent agreement with our results.

7. NATURE OF THE SHOCK FRONTS POWERING THE EMISSION LINES

There are at least two significant theoretical models that predict the structure (density and temperature) and emission behind radiative shocks comparable to those that seem to be occurring in the molecular supernova remnants we observed. One model, by Hollenbach & McKee (1989, hereafter HM89), includes an extensive network of chemical reactions and detailed treatment of the dynamics of the postshock gas (from Hollenbach & McKee 1979). The other model, by Hartigan, Raymond, & Hartmann (1987, hereafter HRH87), includes more ionization states and more ultraviolet and optical lines. We will use the HM89 model as a benchmark, and we will use the [O I] 63 μm line as the normalizing factor. In the HM89 model, the 63 μm line is a significant coolant and should reliably indicate the total energy passing through the shock. Based on the observed width of the line (§ 2.3), we consider the models with shock velocity $V_s = 100$ km s^{-1}. The HM89 model at that velocity that matches the observed [O I] 63 μm brightness has preshock density $n_0 = 10^3$ cm^{-3}. Such a preshock density is reasonable considering that we are observing shocks into molecular clouds. This shock corresponds to what we called "region M" (§ 4.2), although we suggested a somewhat lower preshock density of 10^2 cm^{-3} for this shock. In fact we do not directly measure n_0 and instead estimated it from the density in the emitting region, so a higher n_0 could be consistent with the observations. The compression by the shock depends on many unknown factors, including the strength of the preshock magnetic field.

Before stepping through the comparison of more observed results to the models, we should clarify that the models are themselves significantly different. The physics of shock fronts, especially into dense gas and dust clouds, with so many modes of energy release and interaction, is exceedingly complex and cannot be expected to be accurately predicted by a simple theoretical model. Let us compare the HM89 and HRH87 models for $n_0 = 10^3$ cm^{-3} and $V_s = 100$ km s^{-1}. The HRH87 model is called D100 in their paper. The magnetic field is negligible in the D100 model, but comparing the E100 and B100 models it appears that a stronger magnetic field makes relatively little difference in predicted line brightness within the context of the HRH87 model. Comparing the line brightnesses between the HM89 and HRH87 models, it is clear that there are very significant differences. An extreme case is the [O I] 6300 Å line, which is very bright in the HM89 model but weak in the HRH87 model; the difference is a factor of about 8. A significant part of the difference could be neglect of the higher ionization states in the HM89 model; we suspect the [O II] and [O III] optical lines are much brighter than [O I]. Other significant differences are the importance of Lyα, many high-excitation ultraviolet lines, and the 2-photon continuum; all of these are very bright in the HRH87 model. Part of the difference could be neglect of the radiative transfer through dust in the HRH87 model; we expect most of the ultraviolet photons are absorbed by the cooler layers of the postshock gas and dust or by the remaining unshocked gas and dust.

Comparing our observations to the theoretical shock models, we reach the following conclusions:

Dust emission.—We observe a far-infrared continuum toward the shock fronts, in excess of what we would expect from dust in the quiescent preshock gas. The dust has a color temperature distinctly warmer than dust in molecular or atomic clouds. This could be due to significant collisional or radiative heating in the postshock gas raising the equilibrium temperature of the grains, or it could be due to a significant difference in the size distribution of the postshock grains. Indeed, the postshock size distribution is predicted to be significantly different because the larger grains are shattered (Jones et al. 1996). The HM89 model predicts too little [Fe II] 26 μm and [Si II] 35 μm emission by about a factor of 10. This is probably due to treatment of dust destruction: the elemental abundances in the HM89 model are set at depleted cosmic abundances typical of what may occur in the preshock gas, while dust destruction is now predicted to be significant at these shock velocities (Jones et al. 1996). The HM89 model predicts some infrared continuum, but its flux is weaker than the [O I] 63 μm line, which does not agree with our observations: we find that the continuum flux is much greater than that of any of the emission lines. The HRH87 is on the opposite extreme: they use the entire cosmic abundance in the gas phase, implicitly

assuming complete destruction of the dust and predicting no infrared continuum.

Infrared versus ultraviolet.—The infrared emission escapes from the shocks and arrives at our telescopes, while the ultraviolet (and optical) emission either never escapes the shock or is absorbed before reaching us. The HRH87 model predicts copious ultraviolet emission, with the strongest emission (in order of brightness) arising from Lyα, 2-photon continuum, C III 977 Å, and He II 304 Å. The sum of the five infrared lines they report is still 20 times weaker than Lyα and 3 times weaker than just the He II 304 Å line. Thus, ultraviolet lines (and 2-photon continuum) are by far the dominant cooling behind radiative shocks according to the HRH87 model. On the other hand, the HM89 model predicts a significantly different spectrum, with relatively brighter optical and infrared lines. The brightest line in the HM89 model is the optical [O I] 6300 Å line, followed by Hα and comparable brightnesses of infrared [O I] 63 μm, optical [S II] 6731 Å and [N II] 6560 Å, and ultraviolet C II] 2326 Å lines. Remarkably, the brightness of the C II] 2326 Å and [O II] 3726+3729 Å lines, and Hα and Hβ, agree for the two models, but there are many brighter ultraviolet lines in the HRH87 model. The difference between the two models is at least partially due to the different assumptions about dust grains. The HRH87 model has no dust grains, so that ultraviolet transitions that are optically thick can scatter from ion to ion and eventually escape the shock or have a quantum decay into two photons. If dust grains were included, the ultraviolet photons would not last long before being absorbed. The ultraviolet photons are produced in a thin layer behind the shock, and their energy would heat the surrounding gas, as a radiative precursor into the preshock gas and as an enhanced radiation field in the cooler layers of the postshock gas. In the HM89 model, the radiative transfer does take into account absorption of the ultraviolet lines by dust grains (Hollenbach & McKee 1979), which explains why this model predicts much weaker ultraviolet emission than the HRH87 model. Our detection of a far-infrared continuum suggests that the models must include the effects of dust on the ultraviolet photons.

Molecules.—We detected both the *S*(3) and *S*(9) lines of H_2 (§ 2.2), as well as OH and weak H_2O emission (Reach & Rho 1999). The model of HRH87 does not include molecules, so we will not discuss it here. The model of HM89 includes a chemical reaction network, and they predict the brightness of the *S*(3) and *S*(9) lines to be 9×10^{-6} and 8×10^{-5} ergs s^{-1} cm^{-2} sr^{-1}, respectively. The predicted brightness of the *S*(9) line is about half of what we observed, suggesting that a significant fraction of the *S*(9) line could be produced by a J-type shock. However, the predicted brightness of the *S*(3) line is far lower than we observed. Indeed, for all four of the molecular shocks we observed, the *S*(3) line is brighter than the *S*(9) line; this is contrary to the model, which predicts *S*(3) about 10 times weaker than *S*(9). Instead, it appears that a denser, nondissociating shock is required to explain the *S*(9) line brightness. This picture agrees with presence of a preshock cloud with a range of densities, as shown in our cartoon model. Therefore, it appears that the shock models cannot simultaneously predict both the ionic lines and (all of) the molecular lines with $n_0 = 10^3$ cm^{-3} and $V_s = 100$ km s^{-1}. Instead, it appears that a denser, nondissociating shock is required to explain the *S*(3) line brightness.

To explain the brightness and excitation of the OH and H_2O emission, and the $\sim$30 km s^{-1} width of the CO and CS lines, we suggested C-type shocks into gas with density greater than 10^4 cm^{-3} (Reach & Rho 1998, 1999). Models for such shocks were developed by Draine et al. (1983, hereafter DRD). For $n_0 = 10^4$ cm^{-3} and $V_s = 30$ km s^{-1}, the DRD models predict that H_2 is the dominant coolant, with the brightest lines being *S*(3) and *S*(5). In the DRD model, the *S*(9) line is about 10 times weaker than the *S*(3) line. Given that we observe *S*(3) and *S*(9) lines of comparable brightness, it appears that we are required to have the bulk of the *S*(3) line arise from a C-type shock and part of the *S*(9) line arise from a J-type shock. The observed surface brightness of the *S*(3) line is lower than the predicted brightness from the DRD model ($I_{\rm pred} = 3 \times 10^{-3}$), but that could be due to beam dilution of small, dense clumps that produce the C-type shock.

Comparison to a model of W44.—Two recent papers by Cox et al. (1999) and Shelton et al. (1999) presented a model for the remnant W44. In this model, all observed properties of the remnant, from radio emission to γ-rays, and specifically including the infrared lines, are produced by a blast wave into a smooth medium with a density of 6 cm^{-3}. This model is in marked contrast to the one we presented here, with preshock densities ranging from less than 1 to more than 10^2 cm^{-3}, and some discussion may help to resolve confusion about how they could both be explaining the same data. First, we note that the evidence for molecular cloud interaction is very strong. Shocked CO line with widths of $\sim$30 km s^{-1} were revealed by Seta et al. (1998) and ourselves (this paper, Fig. 7). Second, we note that the uniform preshock conditions in the Cox et al. model are not realistic in a large region of the multiple-phase interstellar medium.

In our model, we attribute the molecular line observations of W44, including H_2 near-infrared emission (Seta et al. 1998), infrared CO lines (Reach & Rho 1998), wide millimeter CO and other lines (Seta et al. 1998), and radio OH 1720 MHz masers (Claussen et al. 1997), to dense, shocked gas. These lines cannot be produced by an ionized low-density postshock region. The analogy to IC 443 is useful—W44 is very similar in many regards, with similar brightnesses of the 63 μm line and brightnesses and widths of the millimeter-wave CO (and other) lines—and few would deny that IC 443 is interacting with a molecular cloud. Finally, the observed brightness of the [O I] 63 μm line cannot easily be explained by a low-density medium, in contrast to the discussion claimed by Cox et al. (1999). The excitation of [O I] evidenced by the 145/63 μm ratio requires a higher density region (Fig. 8). Obviously, [O I] also requires a neutral region, for if the H is ionized the O will also be ionized. The observed lines were so "shockingly" bright that we concluded immediately that they were due to a dense shock (Reach & Rho 1996). In this paper we considered a wide range of densities and ruled out the low densities because (1) they are inconsistent with the line ratios, and (2) the path length required through a low-density gas would be longer than the remnant size in order to build up enough column density to produce the observed line brightness. Cox et al. reduced the brightness of the 63 μm by a factor of 100 to match their models. One of the reduction factors is a factor of 10 to match the estimated average over the entire remnant. Another factor applied by Cox et al. was to enhance their prediction because of limb brightening and local rippling of the shell. While this is perfectly reasonable, this correction was applied to the low-resolution 63 μm line observations, which trace relatively

cool gas, and not to the higher resolution Hα observations (Giacani et al. 1997), which trace warmer gas that might be even more edge brightened. All of these factors probably cancel out to first order when the average over our large beam is made, so that the [O I]/Hα ratio is not matched by their model.

The truth is probably that there were both high- and low-density regions in the interstellar medium around the W44 progenitor star (as considered in this paper and by Chevalier 1999). The particular lines of sight studied in this paper are centered on a special regions, where evidence for a dense shocks are overwhelming. Away from these positions, it is likely that the lower density shocks contribute some of the low-level 63 μm emission. In Figure 9, we are pointed right at a region C clump, while the average over a large region would include different regions in different proportions. Because the 63 μm line brightness is expected to scale approximately as $n_0 V_s$ (HM89), the denser regions contribute relatively more to the observed brightness, when they are present. Further observational work may be able to separate the dense shocked gas from the more rarefied and widespread interclump gas, using imaging to resolve the clumpy spatial distribution and spectroscopy to separate the narrower line widths.

8. CONCLUSIONS

Based on *ISO* spectroscopic observations of supernova remnants interacting with molecular clouds, we found evidence for a wide range of pre- and postshock conditions; these properties are summarized in Table 5 and illustrated in Figure 9. Of the three density regimes that we identified, most of the infrared emission arose from the shocks into moderate-density molecular gas ("region M"). The energy of these shocks is radiated via continuum emission from surviving dust grains and [O I] 63 μm and [Si II] and other infrared atomic fine-structure lines. The dust continuum was difficult to separate from the far-infrared emission from cold, unrelated dust, but the shocked dust was evident at 80–100 μm as a warmer component of the spectrum. Some of the dust grains must have been destroyed, because we observe bright emission lines from dust "vapors," including the [Fe II] 26 μm line. To produce the observed line dust vapor lines, we require that $\frac{1}{3}$ of the Si and Fe-bearing dust mass was vaporized in the shocks. Using the Fabry-Perot observations, the width of the 63 μm line was found to be ~ 100 km s^{-1}. Theoretical models can reproduce the brightness of the 63 μm line with such shock velocities and the properties of "region M" (Hollenbach & McKee 1989); theoretical models can also reproduce the observed amount of grain destruction (Jones et al. 1996). Higher density gas was required to explain the bright H_2 line emission, leading to our "region C," for clumps. Lower density gas was required to explain the higher ionization lines, leading to our "region A," for atomic gas.

A general conclusion from these observations is that molecular shock fronts are copious producers of infrared emission. We anticipate many applications of these types of observations for further understanding the nature of molecular supernova remnants, such as the fate of dense clumps, the fate of dust grains, and the effect of cooling on the remnant evolution. In turn, these studies can elucidate, to some extent, the nature of the molecular clouds before the shocks. If molecular clouds were uniform, or nearly so, then we would expect an orderly progression of preshock to postshock gas, with radiative coolants characteristic of a single shock velocity. On the contrary, we observe emission from coolants as diverse as multiatom molecules, multiply ionized atoms, and dust grains and their vapors.

We would like to thank Pierre-Olivier Lagage for helpful discussions in interpreting atomic fine-structure lines, and we thank Emmanuel Caux, Steve Lord, and Sergio Molinari for clarifying details of the LWS instrument and calibration.

REFERENCES

Anders, E., & Grevesse, N. 1989, Geochim. Cosmochim. Acta, 53, 197
Arendt, R. G. 1996, ApJS, 70, 181
Arikawa, Y., Tatematsu, K., Sekimoto, Y., & Takahashi, T. 1999, PASJ, 51, L7
Becklin, E. E. 1997, in The Far-Infrared and Submillimeter Universe, ed. G. Pilbratt, S. Volonte, & A. Wilson (ESA SP-401; Noordwijk: ESA), 201
Blum, R. D., & Pradhan, A. K. 1992, ApJS, 80, 425
Chevalier, R. A. 1999, ApJ, 511, 798
Claussen, M. J., Frail, D. A., Goss, W. M., & Gaume, R. A. 1997, ApJ, 489, 143
Clegg, P. E., et al. 1996, A&A, 315, L38
Cox, D. P., Shelton, R. L., Maciejewski, W., Smith, R. K., Plewa, T., Pawl, A., & Rózyczka, M. 1999, ApJ, 524, 179
de Graauw, T., et al. 1996, A&A, 315, L49
Désert, F.-X., Boulanger, F., & Puget, J.-L. 1990, A&A, 237, 1
Draine, B. T., & Lee, H. M. 1985, ApJ, 285, 89
Draine, B. T., Roberge, W. G., & Dalgarno, A. 1983, ApJ, 264, 485 (DRD)
Fitzpatrick, E. L. 1996, ApJ, 473, L55
Frail, D. A., Goss, W. M., Reynoso, E. M., Giacani, E. B., Green, A. J., Otrupcek, R. 1996, AJ, 111, 1651
Froese Fischer, C. 1983, J. Phys. B, 16, 157
Giacani, E. B., Dubner, G. M., Kassim, N. E., Frail, D. A., Goss, W. M., Winkler, P. F., & Williams, B. F. 1997, AJ, 113, 1379
Hartigan, P., Raymond, J., & Hartmann, L. 1987, ApJ, 316, 323 (HRH87)
Hollenbach, D. J., & McKee, C. F. 1979, ApJS, 41, 555
———. 1989, ApJ, 342, 306 (HM89)
Hollenbach, D. J., Werner, M. W., & Salpeter, E. E. 1971, ApJ, 163, 165
Jones, A. P., Tielens, A. G. G. M., & Hollenbach, D. J. 1996, ApJ, 469, 740
Kessler, M. F., et al. 1996, A&A, 315, L27
Koo, B.-C., & Heiles, C. 1995, ApJ, 442, 679
Krueger, T. K., & Czyzak, S. J. 1970, Proc. R. Soc. London A, 318, 531
Lagache, G., Abergel, A., Boulanger, F., & Puget, J.-L. 1998, A&A, 333, 709
Launay, J. M., & Roueff, E. 1977, A&A, 56, 289
Liu, X.-W., et al. 1996, A&A, 315, L257
Lockett, P., Gauthier, E., & Elitzur, M. 1999, ApJ, 511, 235
Mendoza, C., & Zeippen, C. J. 1982, MNRAS, 199, 1025
Nussbaumer, H., & Storey, P. J. 1982, A&A, 113, 21
Oliva, E., Lutz, D., Drapatz, S., & Moorwood, A. F. M. 1999a, A&A, 341, L75
Oliva, E., Moorwood, A. F. M., Drapatz, S., Lutz, D., & Sturm, E. 1999b, A&A, 343, 943
Pickett, H. M. Poynter, R. L., Cohen, E. A., Delitsky, M. L., Pearson, J. C., & Müller, H. S. P. 1996, Submillimeter, Millimeter, and Microwave Spectral Line Catalog: Revision 4 (JPL Publ. 80-23; Pasadena: JPL)
Poglitsch, A. 1997, in The Far-Infrared and Submillimeter Universe, ed. G. Pilbratt, S. Volonte, & A. Wilson (ESA SP-401; Noordwijk: ESA), 25
Reach, W. T., & Boulanger, F. 1998, in The Local Bubble and Beyond, ed. D. Brietschwerdt, M. J. Freyburg, & J. Trümper (Berlin: Springer), 353
Reach, W. T., & Rho, J.-H. 1996, A&A, 315, L277 (Paper I)
———. 1998, ApJ, 507, L93
———. 1999, ApJ, 511, 836
Reach, W. T., et al. 1995, ApJ, 451, 188
Rho, J.-H. 1995, Ph.D. thesis, Univ. Maryland
Rho, J.-H., & Petre, R. 1998, ApJ, 503, L167
Rho, J., Jarrett, T., Cutri, R., Reach, W., & van Dyk, S. 2000, ApJ, submitted
Richter, M., Graham, J. R., & Wright, G. S. 1995, ApJ, 454, 277
Savage, B. D., & Sembach, K. R. 1996, ARA&A, 34, 279
Schmutzler, T., & Tscharnuter, W. M. 1993, A&A, 273, 318
Seta, M., et al. 1998, ApJ, 505, 286
Shelton, R. L., Cox, D. P., Maciejewski, W., Smith, R. K., Plewa, T., Pawl, A., & Rózyczka, M. 1999, ApJ, 524, 192
Spitzer, L. 1978, Physical Processes in the Interstellar Medium (New York: Wiley)
Wardle, M. 1999, ApJ, 525, L101
Wild, W. 1995, The 30 m Manual: A Handbook for the IRAM 30 m Telescope (Granada: IRAM)

THE ASTROPHYSICAL JOURNAL, 558:943, 2001 September 10

ERRATUM

In the paper "Infrared Spectroscopy of Molecular Supernova Remnants" by William T. Reach and Jeonghee Rho (ApJ, 544, 843 [2001]), there is a typographical error in Table 5. The shock velocity into the region C clumps should be 20 km s^{-1}, not 200 km s^{-1}. A corrected version of the table is given below.

TABLE 5

PHYSICAL PROPERTIES OF THE THREE POSTSHOCK EMITTING REGIONS

	PRESHOCK		POSTSHOCK			
REGION	n_0 (cm^{-3})	V_s (km s^{-1})	n (cm^{-3})	T (K)	N (cm^{-2})	INFRARED COOLANTS
A (atomic).....	<1	500	8	3000	10^{20}	O III, N III
M (molecular).....	10^2	100	3×10^3	600	10^{21}	O I, Si II, Fe II, N II, H_2 $S(9)$
C (clump).....	10^4	20	4×10^5	200	10^{22}	CO, H_2O, OH, H_2 $S(3)$